

Consistent Video Instance Segmentation with Inter-Frame Recurrent Attention

Quanzeng You Jiang Wang Peng Chu Andre Abrantes Zicheng Liu
 Microsoft Cloud & AI
 {qyou, jiangwang, pengchu, abranes, zliu}@microsoft.com

Abstract

Video instance segmentation aims at predicting object segmentation masks for each frame, as well as associating the instances across multiple frames. Recent end-to-end video instance segmentation methods are capable of performing object segmentation and instance association together in a direct parallel sequence decoding/prediction framework. Although these methods generally predict higher quality object segmentation masks, they can fail to associate instances in challenging cases because they do not explicitly model the temporal instance consistency for adjacent frames. We propose a consistent end-to-end video instance segmentation framework with Inter-Frame Recurrent Attention to model both the temporal instance consistency for adjacent frames and the global temporal context. Our extensive experiments demonstrate that the Inter-Frame Recurrent Attention significantly improves temporal instance consistency while maintaining the quality of the object segmentation masks. Our model achieves state-of-the-art accuracy on both YouTubeVIS-2019 (62.1%) and YouTubeVIS-2021 (54.7%) datasets. In addition, quantitative and qualitative results show that the proposed methods predict more temporally consistent instance segmentation masks.

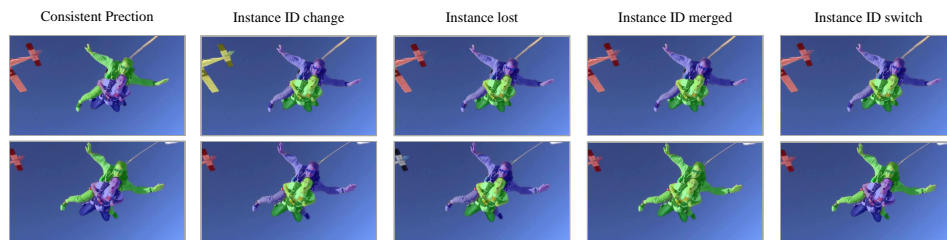


Figure 1: Examples of temporally consistent and inconsistent VIS results. Different mask colors represent different instance identities. The left-most column is the consistent result. Remaining columns are common inconsistent cases.

1 Introduction

Video instance segmentation (VIS) [31] is an emerging task in computer vision. It aims at simultaneously segmenting and tracking object instances in videos. Compared to image instance segmentation methods [10, 4, 19], VIS is more challenging because it does not only require predicting accurate segmentation results for each frame, but also needs to consistently associate the object instances across multiple frames.

Previous VIS methods either independently segment each frame and associate per-frame instances [31, 3, 15, 5, 32], or predict the clip-level instance masks by taking the whole clip as input [1, 28] in an end-to-end manner. Per-frame methods are usually more efficient, while end-to-end per-clip

methods generally achieve better accuracy because they can predict the instance segmentation masks based on information from the whole video clip. Recent methods like VisTR [28], IFC [13], and Mask2Former [8, 7] demonstrate superior accuracy of end-to-end per-clip methods.

These end-to-end per-clip methods adopt a transformer-based end-to-end instance segmentation framework, where one object query is responsible for predicting the object category and segmentation masks of one instance in a video clip. The object category is predicted from the object query through a fully connected network. The segmentation masks of an instance are predicted by convolving the frame features independently with a dynamic kernel that is generated from the object query using a fully connected network and shared across all the frames.

However, we observe that the end-to-end per-clip methods generally cannot maintain temporal instance consistency under challenging conditions, such as overlapping object instances or multiple object instances with the same category (see Figure 1 for examples), because they do not model the relationship of the instance segmentation masks in adjacent frames explicitly. Figure 1 demonstrates common temporal inconsistencies in VIS. The left-most column shows the consistent ground-truth identities and masks for three instances. The remaining columns demonstrate typical inconsistent VIS results, including identity change, instance lost, instance merge and instance identities switch. In videos, the adjacent frames are highly correlated, because the appearance and location of an object instance usually remain consistent in adjacent frames. Incorporating this information explicitly is critical to achieve temporal instance consistency. In this work, we propose an Inter-Frame Recurrent (IFR) attention framework to effectively model the correlation of adjacent frames, together with object appearance and clip-level global context.

In our IFR framework, we have two types of queries. *Clip-level* queries predict object categories and summarize clip-level instance information. *Frame-level* queries predict the instance segmentation masks for the corresponding frames, and they model the specific information about each frame. Several layers of IFR attention modules iteratively update clip-level and frame-level queries to model the temporal relationship. An IFR attention module takes the frame-level queries of the previous frame, the clip-level queries, and the features of the current frame as inputs, and outputs the frame-level queries of the current frame through cross-attention and self-attention modules. The IFR attention module is capable of modeling both the relationship of the object instances in adjacent frames, as well as the relationship of the frame-level and clip-level object instances information. The clip-level queries aggregate the knowledge from all the frames by attending to all frame-level queries. Then, the IFR attention modules in the next layer will utilize these clip-level queries as the clip-level query inputs. We also design an auxiliary loss where the frame-level queries predict the masks of the same instance in other frames to further encourage temporal information propagation.

The proposed framework is simple yet effective as it models the appearance of the instances for each frame, the temporal correlation of the instances, and the clip-level global information. Compared with recent end-to-end approaches that only use global queries [8] for instance segmentation, our design leads to significantly more consistent temporal instance segmentation mask predictions, because it explicitly models the correlation of instances in adjacent frames through the IFR attention module.

By using this framework, our approach sets the new state of the arts on both YouTubeVIS-2019 and YouTubeVIS-2021 datasets. In addition, we show, both quantitatively and qualitatively, that the proposed method generates more consistent instance segmentation masks while being more robust across multiple training runs. We also propose a test-time augmentation (TTA) method to further boost the accuracy and robustness of the proposed method. We believe that the significantly improved temporal instance consistency of the proposed framework is not only beneficial to the overall instance segmentation accuracy, but also critical to the perceived quality of video instance segmentation.

2 Related work

Image instance segmentation Image instance segmentation attempts to classify an object’s semantic category and recognize its pixels for a given image. One popular image instance segmentation method is a two-stage method called Mask R-CNN [10], which detects each instance first and then recognizes the belonging pixels. Recently, due to their simplicity and competitive performance, one stage approaches [26, 24] are gaining popularity. In particular, the introduction of dynamic kernels [24] significantly boosted the performance of the one-stage approach [27]. More recently, the employment of Transformers [25] and bipartite matching based ground truth assignments led to the

success of end-to-end object detection [6, 33, 18]. In end-to-end object detection, each object query predicts both the category label and the bounding box of an object. This mechanism has been applied to end-to-end instance segmentation [9, 12, 8] as well. In these approaches, object queries predict the semantic labels of the instances and produce dynamic kernels for mask prediction. Together with more powerful transformer-based backbones [20], these approaches set the new state of the art on image instance segmentation.

Video instance segmentation Video instance segmentation was introduced in [31] and involves segmenting instances at each frame while also tracking them across frames. Early studies [31, 3, 15, 5, 32] independently locate instances in each frame and attempt to associate the instances across frames with tracking methods. These per-frame based approaches are also known as tracking-by-detection. Later, STEM-Seg [1] learns spatio-temporal embeddings from video clips, which are clustered and linked across frames to produce video-level instances. This approach is end-to-end trained, without an explicit tracking mechanism. Meanwhile, VisTR [28] builds their framework upon Transformers [25]. Inspired by the end-to-end image instance segmentation, the instance segmentation results of each frame are produced by frame-level queries. Then, similarity learning is employed to group frame-level queries for instance tracking. STEM-Seg and VisTR also employ a clip matching mechanism for inference in long videos. To avoid the clip matching and computational complexity, Propose-Reduce [16] chooses to generate instance segmentation results on selected keyframes, and propagate the results to all the other frames. Each non-key frame receives and reduces the results from all keyframes to produce its result. This strategy balances performance and speed. The potential of end-to-end approaches is further explored in the recent state-of-the-art models [13, 29, 8]. Inter-Frame Communication (IFC) [13] employs compact memory tokens to efficiently fuse all the frame tokens obtained from the transformer encoder. The output of the encoder is then fed to the decoder for video instance segmentation. SeqFormer [29] employs frame-level box queries on each frame to generate frame-level mask queries for segmentation. The learning contains both mask prediction and object detection tasks. Mask2Former [8] directly uses all spatio-temporal tokens as inputs to the decoder to generate global mask queries, achieving a new state of the art.

3 Approach

Our approach is based on the end-to-end framework that was initially proposed for object detection [6]. Video instance segmentation involves two essential tasks: instance segmentation of each frame and instance association across frames. End-to-end approaches are able to achieve superior accuracy, because they allow both tasks to use all the information of the whole video by modeling the two essential tasks together. However, we found that state-of-the-art video instance segmentation methods exhibit temporally inconsistent instance segmentation masks because the instance association task is not well modeled. In this paper, we propose an Inter-Frame Recurrent (IFR) attention framework to significantly improve the modeling of instance association across frames in Transformer-based end-to-end video instance segmentation methods. Similar to [8], we employ a multi-scale Deformable encoder to fuse the pyramid of features from the backbone. The fused pyramid of features is used in IFR attention module to generate frame-level queries for mask prediction and clip-level queries for instance category classification. The IFR attention module simultaneously models the object appearance in each frame, the relationship of adjacent frames, and the clip-level context. Thus, it more effectively models instance association tasks by encouraging temporally consistent instance segmentation masks. Figure 2 shows the main components of the framework.

3.1 Model framework

Backbone The backbone generates frame-level appearance features for each video frame. Following the recent end-to-end work on video instance segmentation, we adopt image-based backbones for feature extraction. For an image I with size of $H \times W$, the backbone produces a pyramid of feature maps with sizes of $H/4 \times W/4$, $H/8 \times W/8$, $H/16 \times W/16$ and $H/32 \times W/32$.

Multi-scale transformer encoder Multi-scale transformer encoder fuses the information across the pyramid of feature maps in end-to-end instance segmentation tasks [12, 29, 8]. In this work, we adopt the memory-efficient multi-scale Deformable Transformer [33] to fuse the pyramid of features, similar to [8]. The outputs of the multi-scale Deformable Transformer is a fused pyramid of features

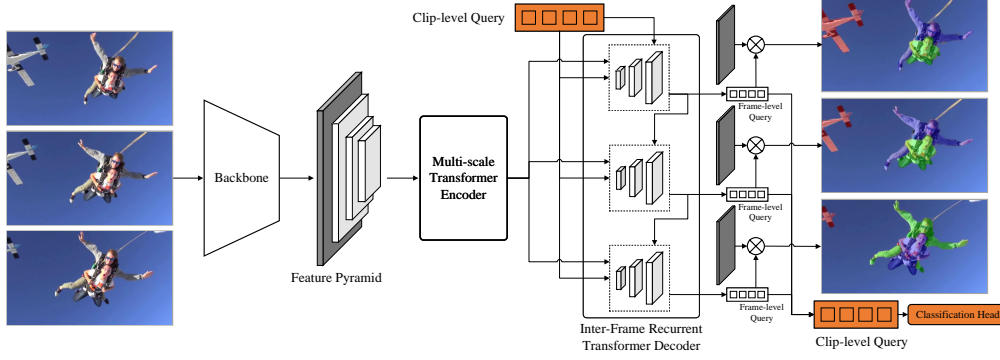


Figure 2: Illustration of our framework. Following recent studies, we also adopt multi-scale encoder to fuse multi-scale features. For each frame, we learn frame-level queries for mask prediction. The video-level queries, which aggregate the information across different frames, are utilized for the instance classification task.

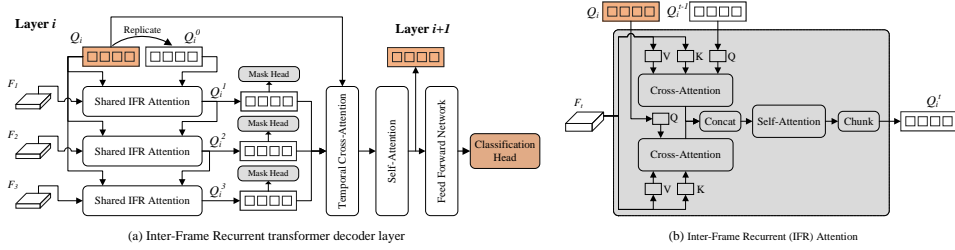


Figure 3: Architecture of our Inter-Frame Recurrent transformer decoder (for simplicity, we only show a clip of three frames). In the beginning stage of the i -th layer, we employ Inter-Frame Recurrent (IFR) attention to construct the *frame-level* queries to predict the instance mask at each frame. The frame-level queries are aggregated with the temporal cross-attention module to generate the clip-level queries for video instance classification.

of the same size as the input. Each scale of the fused pyramid of features is input to the instance segmentation decoder in a layer-by-layer fashion [8, 7].

Inter-frame recurrent transformer decoder For end-to-end transformer-based video instance segmentation, object queries play a critical role in modeling both instance appearance and temporal instance relationship. We propose the inter-frame recurrent transformer decoder as shown in Figure 3.

For the i -th decoder layer, the set of *clip-level* queries are denoted as Q_i . Each clip also comes with n sequential *frame-level* feature maps (F_1, F_2, \dots, F_n). The *frame-level* queries for the t -th frame are denoted by Q_i^t . Inter-frame recurrent attention module employs the *clip-level* queries Q_i , the feature map F_t , and the previous frame’s *frame-level* queries Q_i^{t-1} to compute *frame-level* queries Q_i^t for mask prediction. The multi-head attention module, with hidden dimension of d , is employed

$$\text{Attn}(Q, K, V) = \text{Softmax} \left(\frac{(QK^T) \odot M}{\sqrt{d}} \right) V, \quad (1)$$

where M is an optional binary attention mask tensor and \odot represents the element-wise multiplication between two tensors.

In particular, given current feature map F_t , cross-attention module is utilized to compute the updated frame-level and clip-level queries from Q_i and Q_i^{t-1} . Then, both groups of queries are concatenated to form $Q_i^{t'}$:

$$Q_i^{t'} = [\text{Attn}(Q_i^{t-1}, F_{T+t}W^K, F_{T+t}W^V), \text{Attn}(Q_i, F_{T+t}W^K, F_{T+t}W^V)]. \quad (2)$$

$Q_i^{t'}$ goes through a self-attention module. The eventual queries Q_i^t are obtained by splitting $Q_i^{t'}$ and keeping the first group of queries.

$$Q_i^t = \text{Chunk}(\text{Attn}(Q_i^{t'}, Q_i^{t'}W'^K, Q_i^{t'}W'^V)). \quad (3)$$

In this way, the frame-level queries Q_i^t do not only utilize the appearance features from F_t and clip-level features, but also leverage the local temporal information from Q_i^{t-1} . The local temporal information is crucial for encouraging temporally consistent instance segmentation mask predictions. At the start of a clip $t = 1$, we initialize the previous frame-level query Q_i^0 to be a copy of clip-level query Q_i (as shown in Figure 3).

The above steps compute the *frame-level* queries for each frame. Next, we update *clip-level* queries Q_i by aggregating the knowledge in all the frame-level queries $\mathbf{Q} = \{Q_i^1, \dots, Q_i^n\}$. This is achieved by using temporal cross-attention, where Q_i s are the query, and all frame-level queries \mathbf{Q} are used as key and value. Another self-attention module on the output of the temporal cross-attention generates the clip-level queries Q_{i+1} . Q_{i+1} is used for the instance classification task, as well as the clip-level queries for the $(i + 1)$ -th layer.

3.2 Instance segmentation training loss

Similar to previous work, one ground-truth video instance is associated with one object query with Hungarian algorithm. The cost of assigning i -th ground-truth instance to π_i -th clip-level query is

$$\mathcal{C}_{\text{match}} = -\lambda_c \hat{p}_{\pi_i}(c_i) + \lambda_m \mathcal{C}_m(m_i, \hat{m}_{\pi_i}) + \lambda_d (1 - \text{DICE}(m_i, \hat{m}_{\pi_i})), \quad (4)$$

where \hat{p}_{π_i} is the predicted classification probability of clip-level query π_i , $\mathcal{C}_m(\cdot, \cdot)$ computes the binary cross-entropy between predicted and ground-truth masks, and the DICE is the dice coefficient defined in [21]. The optimal assignment π is computed as minimizing the cost for all M ground-truth instances in a training clip.

Training loss The training loss is similar to the above matching cost. It consists of the classification loss \mathcal{L}_{cls} , the cross-entropy mask loss $\mathcal{L}_{\text{mask}}$ and the DICE loss $\mathcal{L}_{\text{DICE}}$.

As discussed above, Inter-Frame Recurrent attention module is employed to generate *frame-level* queries for mask prediction. Although the information from the other frames in the clip can be propagated through *clip-level* queries and previous frame’s *frame-level* queries, we find it is beneficial to add an auxiliary cross-frame mask prediction loss to further utilize temporal information, where each *frame-level* queries are used to predict the masks of the same instance in the other frames in the same training clip. Our training loss can be represented as:

$$\mathcal{L} = \sum_{i=1}^N \lambda_c \mathcal{L}_{\text{cls}}(c_i, \hat{p}_{\pi_i}) + \mathbb{1}_{c_{\pi_i} \neq \emptyset} [\lambda_m \bar{\mathcal{L}}_m(m_i, \hat{m}_{\pi_i}) + \lambda_D \bar{\mathcal{L}}_D(m_i, \hat{m}_{\pi_i})], \quad (5)$$

where λ_c , λ_m and λ_D are the loss weights, $\mathbb{1}_{c_{\pi_i} \neq \emptyset}$ controls only queries that matched with ground-truth will have mask and DICE loss. For the classification loss \mathcal{L}_{cls} , we employ Focal loss [17], which demonstrates performance gain for instance segmentation as well [33]. Both $\bar{\mathcal{L}}_m$ and $\bar{\mathcal{L}}_D$ consider the cross-frame mask predictions as well. More specifically, we have

$$\bar{\mathcal{L}}_m(m_i, \hat{m}_{\pi_i}) = \sum_{t_1} \left[\mathcal{L}_m(m_i^{t_1}, \hat{m}_{\pi_i}^{t_1}) + \lambda_e \sum_{t_2, t_2 \neq t_1} \mathcal{L}_m(m_i^{t_2}, \hat{m}_{\pi_i}^{t_1}) \right] \quad (6)$$

$$\bar{\mathcal{L}}_D(m_i, \hat{m}_{\pi_i}) = \sum_{t_1} \left[(1 - \text{DICE}(m_i^{t_1}, \hat{m}_{\pi_i}^{t_1})) + \lambda_e \sum_{t_2, t_2 \neq t_1} (1 - \text{DICE}(m_i^{t_2}, \hat{m}_{\pi_i}^{t_1})) \right], \quad (7)$$

where λ_e is the weight for cross-frame mask loss, m_i^t and $\hat{m}_{\pi_i}^t$ are the ground-truth mask of the i -th instance and the matched predicted mask at frame t of the given training clip.

Test time augmentation (TTA) Test time augmentation is widely used in computer vision tasks [14, 11]. TTA feeds multiple augmented testing images or videos to the network to produce multiple predictions for a testing image or video. The final result is obtained by aggregating all the predicted results using a post-processing method, such as Non-Maximum Suppression (NMS) [22] in object detection. For instance segmentation, TTA is rarely applied due to the difficulty in merging multiple results. We propose a TTA mechanism for instance segmentation by applying the matching mechanism in the training stage (Eq. (4)). If we have n different instance segmentation results

$\{R_1, R_2, \dots, R_n\}$ from the same video, we randomly choose one result R_p as the pivot. All other results are matched to R_p based on the matching cost in Eq.(4) so that each instance in R_p is matched to $n - 1$ instances. The aggregated result for an instance contains the averaged classification probabilities and instance mask probabilities for the corresponding n matched instances. A similar strategy was adopted for clip-level instance tracking in [13].

4 Experiments

Following previous studies [31], we evaluate the proposed approach on YouTubeVIS-2019 and YouTubeVIS-2021 datasets (released with Creative Commons Attribution 4.0 License).¹ The two datasets contain similar videos, annotations, and evaluation metrics. YouTubeVIS-2021 contains more videos, improved categories, and roughly twice as much as video instance annotations compared to the 2019 version. We adopt the mean of average precision (AP) over all classes as the main metric, which is similar to the AP metric in image instance segmentation. We also report AP50 and AP75, where IoU thresholds of 0.5 and 0.75 are used when calculating AP respectively, as well as average recall (AR). All the metrics are generated using the official evaluation servers of YouTubeVIS-2019 and YouTubeVIS-2021 datasets.

Table 1: Evaluation results on **YouTubeVIS-2019** validation split.

Method	Backbone	Data	AP	AP50	AP75	AR1	AR10
SeqFormer	ResNet-50	Y + COCO	47.4	69.8	51.8	45.5	54.8
	ResNet-101	Y + COCO	49.0	71.1	55.7	46.8	56.9
Mask2Former	ResNet-50	Y	46.4±0.8	68.0	50.0	-	-
	ResNet-101	Y	49.2±0.7	72.8	54.2	-	-
Ours	ResNet-50	Y	46.5±0.8	68.4	50.1	46.3	55.9
	ResNet-101	Y	49.3±0.4	75.2	59.7	48.5	58.2
SeqFormer*	Swin-L	Y + COCO	59.4	82.1	66.4	51.7	64.4
Mask2Former	Swin-T	Y	51.5±0.7	75.0	56.6	-	-
	Swin-S	Y	54.3±0.7	79.0	58.8	-	-
	Swin-B	Y	59.5±0.7	84.3	67.2	-	-
	Swin-L-200	Y	60.4±0.5	84.4	67.0	-	-
Ours	Swin-T	Y	52.8±0.3	75.2	59.7	50.3	61.7
	Swin-S	Y	56.2±0.1	79.9	62.3	52.5	63.8
	Swin-B	Y	61.3±0.4	84.6	68.4	54.3	66.7
	Swin-L	Y	62.1±0.2	84.9	69.2	55.1	67.1
	Swin-L-200	Y	61.2±0.3	84.6	69.3	54.8	67.3
	Swin-L (TTA)	Y	62.6±0.1	84.8	69.3	55.5	68

*For Swin-L, input resolution is 360 for shorter size, where 480 is used for Mask2Former and our model.

4.1 Training setup

We implement our model based on IFC [13] with Apache 2.0 license and Mask2Former [8] with Creative Commons Attribution-NonCommercial 4.0 International License, using Detectron2 framework [30] under Apache License 2.0. All models are trained with a node of 8 NVIDIA V100 GPUs. Following the common recipe in [13, 7], we initialize our model with weights pre-trained on COCO dataset because both YouTubeVIS2019 and YouTubeVIS2021 datasets are relatively small-scale. Since pretraining the inter-frame recurrent attention modules is not possible with an image instance segmentation dataset, we randomly initialize these modules. During training, we randomly sample clips [13, 7] from each video. The number of frames for each video is set to 2, and the shorter side of the training clip is resized to 360 or 480, following [8]. The learning rate for the backbone is 1/10 of the learning rate of other parts of the network. We follow the same setting in [8]: $\lambda_c = 2$, $\lambda_m = 5$ and $\lambda_D = 5$ in Eq.(5). $\lambda_e = 0.3$ in Eq.(6). During inference, the model takes the whole video and predicts the video instance segmentation for all the frames.

¹<https://youtube-vos.org/dataset/vis/>

4.2 Main results

In this section, we report the results on both YouTubeVIS 2019 and YouTubeVIS 2021 datasets. All metrics are obtained by training our models on the training splits independently five times and averaging the evaluation metrics. We mainly compare with SeqFormer [29] and Mask2Former [8, 7], which are state-of-the-art Transformer-based end-to-end approaches.

YouTubeVIS 2019 results Table 1 summarizes the results on the validation split of YouTubeVIS 2019 dataset. For CNN-based backbone, our results are comparable with SeqFormer [29] and Mask2Former [8]. Our approach demonstrated large performance gains using Swin Transformer [20] backbones. Our experiments also show that the proposed model is able to achieve better performance using fewer queries (100 queries compared to 200 queries in Mask2Former [8]). In particular, our model with Swin-L backbone and 100 queries achieve 62.1 ± 0.2 AP, which is almost 2 percent better than the previous state-of-the-art end-to-end method.

In test time augmentation, we resize the testing videos to four different input resolutions during inference, and average the matched predictions. The ‘‘Swin-L (TTA)’’ is the result of using TTA on Swin-L backbone. The TTA strategy improves AP and reduces the variances of the results.

YouTubeVIS 2021 results YouTubeVIS 2021 is a more challenging updated version of the YouTubeVIS 2019 dataset. The results are summarized in Table 2. Our models demonstrate the best results across all different backbones. Compared with Mask2Former, our model achieves a much smaller variance with higher AP. This dataset is more challenging, thus TTA shows a larger gain compared with the results on YouTube VIS 2019 dataset.

Table 2: Evaluation results on **YouTubeVIS-2021** validation split.

Method	Backbone	Data	AP	AP50	AP75	AR1	AR10
SeqFormer [29]	ResNet-50	Y + COCO	40.5	62.4	43.7	36.1	48.1
Mask2Former	ResNet-50	Y	40.6±0.7	60.9	41.8	-	-
	ResNet-101	Y	42.4±0.6	65.9	45.8	-	-
Ours	ResNet-50	Y	41.8±0.2	63.0	44.9	39.2	48.8
	ResNet-101	Y	42.9±0.1	64.7	46.2	40.0	50.5
SeqFormer	Swin-L	Y+COCO	51.8	74.6	58.2	42.8	58.1
Mask2Former	Swin-T	Y	45.9±0.6	68.7	50.7	-	-
	Swin-S	Y	48.6±0.4	77.2	52.0	-	-
	Swin-B	Y	52.0±0.6	76.5	54.2	-	-
	Swin-L	Y	52.6±0.7	76.4	57.2	-	-
Ours	Swin-T	Y	47.4±0.9	69.2	52.5	41.7	54.3
	Swin-S	Y	49.4±0.2	71.2	54.0	43.5	55.9
	Swin-B	Y	53.9±0.2	76.4	60.2	45.1	58.8
	Swin-L	Y	54.7±0.2	76.8	61.2	44.4	58.6
	Swin-L (200)	Y	54.0±0.1	75.8	60.1	45.2	58.8
	Swin-L (TTA)	Y	55.6±0.05	77.3	61.8	45.7	59.6

4.3 Ablation study for cross-frame mask prediction loss

We perform ablation study for the auxiliary cross-frame mask prediction loss (Eq.(6) and Eq.(7)). To study the impact of this loss, we randomly select 400 videos from the YouTubeVIS2019 training set as the ablation study validation set, and train the proposed model with ResNet-50 backbone using different values of λ_e on the remaining training data. For each λ_e , we run five independent training. The means and variances of the evaluation metrics are visualized in Figure 4. The results suggest that the proposed consistency mask loss can improve the performance of AP compared with the results without using the loss ($\lambda_e = 0$), although a too large λ_e leads to worse results. Overall, the best performance is achieved when $\lambda_e = 0.3$. We choose $\lambda_e = 0.3$ in all of our experiments.

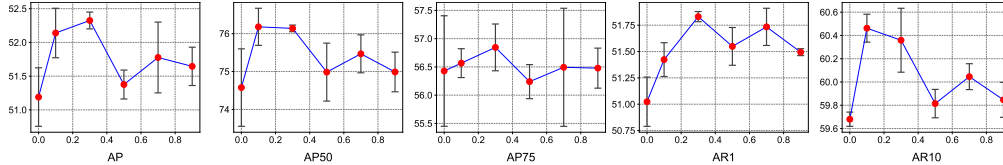


Figure 4: Results of our propose model with different loss weights λ_e (Eq.(6) and Eq.(7)). All models are trained with ResNet-50 as the backbone. For each λ_e , we run five experiments. The mean and variance (indicated by the error bar) of each parameter setting for different metrics are visualized.

4.4 Evaluation of temporal consistency

In this section, we design an experiment to evaluate the temporal consistency of our model through tracking metrics.

We calculate a tight bounding box that encloses each instance mask as the bounding box for each instance object in both the predicted and ground-truth results, and employ the widely used tracking metrics in multiple object tracking (MOT) task [2, 23]. The tracking metrics can characterize the instance-level temporal inconsistency, such as false-positive and false-negative instance tracks. Trajectory ID-related metrics include ID precision (IDP), ID recall (IDR), IDF1, and identity switches between tracklets. Multiple object tracking accuracy (MOTA), which measures the overall accuracy of tracker and detection, is another important metric. We employ the open-sourced implementation² with an IoU threshold of 0.5, which controls the computation of the metrics and is commonly adopted in tracking tasks. We conduct this experiment on the same ablation study data splitting as in Figure 4, because we need to access the ground-truth annotations.

Table 3: Comparison between different approaches in terms of the tracking metrics, which measure the performance of associating instances across frames. We compare the two approaches on both YouTubeVIS (YTVIS) 2019 and YouTubeVIS (YTVIS) 2021 datasets.

Method	Backbone	Dataset	IDF1 \uparrow	MOTA \uparrow	IDP \uparrow	IDR \uparrow	IDs \downarrow
Mask2Former	ResNet-50	YTVIS19	62.4%	14.6	54.7%	74.3%	202
	Swin-L (200)	YTVIS19	66.7%	23.0	57.1%	80.3%	218
Ours	ResNet-50	YTVIS19	72.2%	47.6	74.7%	70.0%	50
	Swin-L	YTVIS19	77.8%	57.5	78.2%	77.4%	48
	Swin-L (200)	YTVIS19	78.3%	58.7	79.2%	77.4%	26
Mask2Former	ResNet-50	YTVIS21	55.1%	-1.6	47.3%	66.2%	790
	Swin-L (200)	YTVIS21	61.7%	14.5	53.0%	73.9%	729
Ours	ResNet-50	YTVIS21	64.1%	36.4	70.1%	59.1%	141
	Swin-L	YTVIS21	70.8%	47.5	74.5%	67.4%	123
	Swin-L (200)	YTVIS21	71.1%	48.7	76.4%	66.4%	94

Table 3 shows the results of Mask2Former and ours with ResNet-50 and Swin-L backbones on both datasets. Our models demonstrate significant improvements in terms of the tracking metrics. The scores on IDF1, IDs and MOTA suggest the effectiveness of our proposed model in terms of preserving consistent identity ID for instances across all the video frames.

4.5 Quantitative results visualization

To visually compare the prediction results of the proposed method and Mask2Former, we select several instance segmentation results, as shown in Figure 5, from both models trained with Swin-L backbone. For the first sequence, both approaches demonstrate consistent video instance prediction results. All instances are accurately segmented within each frame and correctly tracked across frames. For this video, it is easier for the model to predict temporally consistent instances, because all the “deers” stay almost at the same poses with only slight movements. For the second clip, there are multiple “apes”: one sits still, two of them play with each other and the last one walks by. As

²<https://github.com/cheind/py-motmetrics> released under MIT License.

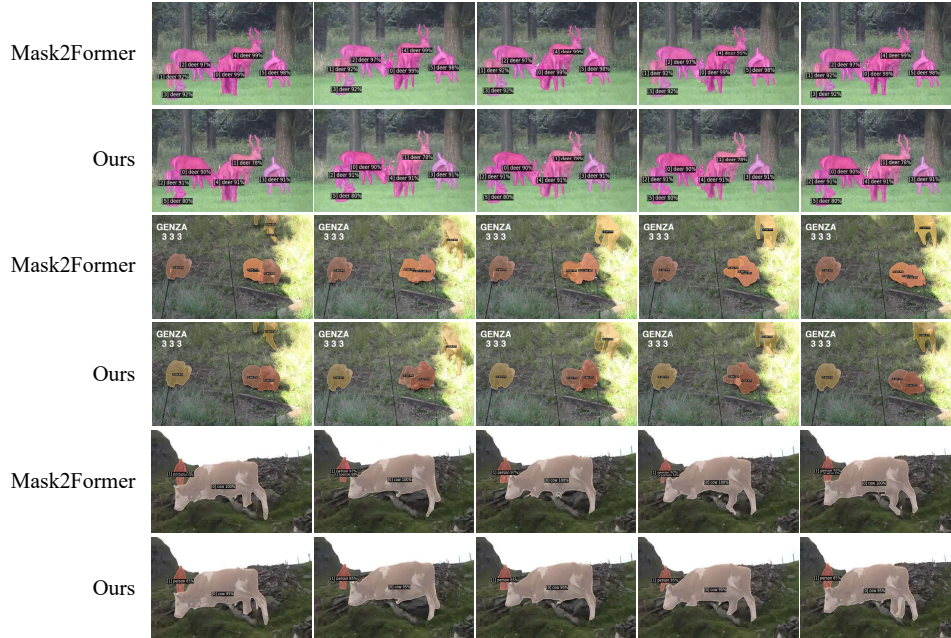


Figure 5: Visualization results of our model and Mask2Former on selected multi-instance sequences. All results are from the model with Swin-L backbone.

suggested by the results, Mask2Former generates duplicate predictions for the walking ape and the two playing apes. The instance IDs for these apes also switched. In comparison, our results assign unique and consistent instance ID for each ape. The last sequence contains two instances with different categories: person and cow. The cow passes by the person. The person is assigned as two different instances by Mask2Former, while our results allocate one instance for the person. In practice, we found that temporal inconsistencies significantly degrade the perceived video segmentation quality, because humans can easily observe these temporal inconsistencies. These results show that our approach can assign consistent instance identities across frames.

4.6 Limitation

Our models are too computationally expensive to be deployed for real-time inference. We can implement per-clip inference, but the speed still cannot meet the requirements of real-time applications.

5 Conclusion

Video instance segmentation is a relatively new vision task. It involves instance segmentation within each frame and instance association across frames. In this work, we attempt to improve the instance association quality by simultaneously employing Inter-Frame Recurrent (IFR) attention for integrating frame-specific features and propagating video-level temporal features. In addition, we also propose to include the cross-frame mask prediction loss for discriminative frame-level query learning. In this way, the proposed approach achieves the new state-of-the-art performance on both YouTubeVIS 2019 and YouTubeVIS 2021 datasets. Inspired by the matching strategy in associating ground truth with each query, we also propose the test time augmentation strategy, which further benefits the inference results. Our work fuses the temporal information for video instance segmentation primarily in the head of the network. In the future, we hope temporal information can be more effectively aggregated in network backbones for dense prediction video tasks. Our models are trained on video data, which may contain social biases and the training process can cause environmental costs. We will examine and alleviate these social impacts in the future.

References

- [1] Ali Athar, Sabarinath Mahadevan, Aljosa Osep, Laura Leal-Taixé, and Bastian Leibe. Stem-seg: Spatio-temporal embeddings for instance segmentation in videos. In *European Conference on Computer Vision*, pages 158–177. Springer, 2020.
- [2] Keni Bernardin and Rainer Stiefelhagen. Evaluating multiple object tracking performance: the clear mot metrics. *EURASIP Journal on Image and Video Processing*, 2008:1–10, 2008.
- [3] Gedas Bertasius and Lorenzo Torresani. Classifying, segmenting, and tracking object instances in video with mask propagation. In *Proceedings of the IEEE/CVF Conference on Computer Vision and Pattern Recognition*, pages 9739–9748, 2020.
- [4] Daniel Bolya, Chong Zhou, Fanyi Xiao, and Yong Jae Lee. Yolact: Real-time instance segmentation. In *Proceedings of the IEEE/CVF international conference on computer vision*, pages 9157–9166, 2019.
- [5] Jiale Cao, Rao Muhammad Anwer, Hisham Cholakkal, Fahad Shahbaz Khan, Yanwei Pang, and Ling Shao. Sipmask: Spatial information preservation for fast image and video instance segmentation. In *European Conference on Computer Vision*, pages 1–18. Springer, 2020.
- [6] Nicolas Carion, Francisco Massa, Gabriel Synnaeve, Nicolas Usunier, Alexander Kirillov, and Sergey Zagoruyko. End-to-end object detection with transformers. In *European conference on computer vision*, pages 213–229. Springer, 2020.
- [7] Bowen Cheng, Anwesa Choudhuri, Ishan Misra, Alexander Kirillov, Rohit Girdhar, and Alexander G Schwing. Mask2former for video instance segmentation. *arXiv preprint arXiv:2112.10764*, 2021.
- [8] Bowen Cheng, Ishan Misra, Alexander G. Schwing, Alexander Kirillov, and Rohit Girdhar. Masked-attention mask transformer for universal image segmentation. 2022.
- [9] Bowen Cheng, Alexander G. Schwing, and Alexander Kirillov. Per-pixel classification is not all you need for semantic segmentation. In *NeurIPS*, 2021.
- [10] Kaiming He, Georgia Gkioxari, Piotr Dollár, and Ross Girshick. Mask r-cnn. In *Proceedings of the IEEE international conference on computer vision*, pages 2961–2969, 2017.
- [11] Kaiming He, Xiangyu Zhang, Shaoqing Ren, and Jian Sun. Deep residual learning for image recognition. In *Proceedings of the IEEE conference on computer vision and pattern recognition*, pages 770–778, 2016.
- [12] Jie Hu, Liujuan Cao, Yao Lu, ShengChuan Zhang, Yan Wang, Ke Li, Feiyue Huang, Ling Shao, and Rongrong Ji. Istr: End-to-end instance segmentation with transformers. *arXiv preprint arXiv:2105.00637*, 2021.
- [13] Sukjun Hwang, Miran Heo, Seoung Wug Oh, and Seon Joo Kim. Video instance segmentation using inter-frame communication transformers. *Advances in Neural Information Processing Systems*, 34, 2021.
- [14] Alex Krizhevsky, Ilya Sutskever, and Geoffrey E Hinton. Imagenet classification with deep convolutional neural networks. *Advances in neural information processing systems*, 25, 2012.
- [15] Chung-Ching Lin, Ying Hung, Rogerio Feris, and Linglin He. Video instance segmentation tracking with a modified vae architecture. In *Proceedings of the IEEE/CVF Conference on Computer Vision and Pattern Recognition*, pages 13147–13157, 2020.
- [16] Huajia Lin, Ruizheng Wu, Shu Liu, Jiangbo Lu, and Jiaya Jia. Video instance segmentation with a propose-reduce paradigm. In *Proceedings of the IEEE/CVF International Conference on Computer Vision*, pages 1739–1748, 2021.
- [17] Tsung-Yi Lin, Priya Goyal, Ross Girshick, Kaiming He, and Piotr Dollár. Focal loss for dense object detection. In *Proceedings of the IEEE international conference on computer vision*, pages 2980–2988, 2017.
- [18] Shilong Liu, Feng Li, Hao Zhang, Xiao Yang, Xianbiao Qi, Hang Su, Jun Zhu, and Lei Zhang. Dab-detr: Dynamic anchor boxes are better queries for detr. In *International Conference on Learning Representations*, 2021.
- [19] Shu Liu, Lu Qi, Haifang Qin, Jianping Shi, and Jiaya Jia. Path aggregation network for instance segmentation. In *Proceedings of the IEEE conference on computer vision and pattern recognition*, pages 8759–8768, 2018.
- [20] Ze Liu, Yutong Lin, Yue Cao, Han Hu, Yixuan Wei, Zheng Zhang, Stephen Lin, and Baining Guo. Swin transformer: Hierarchical vision transformer using shifted windows. In *Proceedings of the IEEE/CVF International Conference on Computer Vision*, pages 10012–10022, 2021.
- [21] Fausto Milletari, Nassir Navab, and Seyed-Ahmad Ahmadi. V-net: Fully convolutional neural networks for volumetric medical image segmentation. In *2016 fourth international conference on 3D vision (3DV)*, pages 565–571. IEEE, 2016.

- [22] Alexander Neubeck and Luc Van Gool. Efficient non-maximum suppression. In *18th International Conference on Pattern Recognition (ICPR'06)*, volume 3, pages 850–855. IEEE, 2006.
- [23] Ergys Ristani, Francesco Solera, Roger Zou, Rita Cucchiara, and Carlo Tomasi. Performance measures and a data set for multi-target, multi-camera tracking. In *European conference on computer vision*, pages 17–35. Springer, 2016.
- [24] Zhi Tian, Chunhua Shen, and Hao Chen. Conditional convolutions for instance segmentation. In *European Conference on Computer Vision*, pages 282–298. Springer, 2020.
- [25] Ashish Vaswani, Noam Shazeer, Niki Parmar, Jakob Uszkoreit, Llion Jones, Aidan N Gomez, Łukasz Kaiser, and Illia Polosukhin. Attention is all you need. *Advances in neural information processing systems*, 30, 2017.
- [26] Xinlong Wang, Tao Kong, Chunhua Shen, Yuning Jiang, and Lei Li. Solo: Segmenting objects by locations. In *European Conference on Computer Vision*, pages 649–665. Springer, 2020.
- [27] Xinlong Wang, Rufeng Zhang, Tao Kong, Lei Li, and Chunhua Shen. Solov2: Dynamic and fast instance segmentation. *Advances in Neural information processing systems*, 33:17721–17732, 2020.
- [28] Yuqing Wang, Zhaoliang Xu, Xinlong Wang, Chunhua Shen, Baoshan Cheng, Hao Shen, and Huaxia Xia. End-to-end video instance segmentation with transformers. In *Proceedings of the IEEE/CVF Conference on Computer Vision and Pattern Recognition*, pages 8741–8750, 2021.
- [29] Junfeng Wu, Yi Jiang, Wenqing Zhang, Xiang Bai, and Song Bai. Seqformer: a frustratingly simple model for video instance segmentation. *arXiv preprint arXiv:2112.08275*, 2021.
- [30] Yuxin Wu, Alexander Kirillov, Francisco Massa, Wan-Yen Lo, and Ross Girshick. Detectron2. <https://github.com/facebookresearch/detectron2>, 2019.
- [31] Linjie Yang, Yuchen Fan, and Ning Xu. Video instance segmentation. In *Proceedings of the IEEE/CVF International Conference on Computer Vision*, pages 5188–5197, 2019.
- [32] Shusheng Yang, Yuxin Fang, Xinggong Wang, Yu Li, Chen Fang, Ying Shan, Bin Feng, and Wenyu Liu. Crossover learning for fast online video instance segmentation. In *Proceedings of the IEEE/CVF International Conference on Computer Vision*, pages 8043–8052, 2021.
- [33] Xizhou Zhu, Weijie Su, Lewei Lu, Bin Li, Xiaogang Wang, and Jifeng Dai. Deformable detr: Deformable transformers for end-to-end object detection. In *International Conference on Learning Representations*, 2020.

A Appendix

A.1 Per-clip inference

Table 4: Evaluation results of using per-clip inference on both datasets of using Swin-L backbone. The clip length $T = v$ indicates per-video inference.

Dataset	Backbone	Clip length (T)	AP	AP50	AP75	AR1	AR10
YTVIS2019	Swin-L	v	62.1±0.2	84.9	69.2	55.1	67.1
	Swin-L (TTA)	v	62.6±0.1	84.8	69.3	55.5	68
	Swin-L-CLIP	2	61.6±0.6	84.3	68.0	54.3	66.0
	Swin-L-CLIP	5	61.8±0.2	85.5	68.0	54.3	65.9
YTVIS2021	Swin-L	v	54.7±0.2	76.8	61.2	44.4	58.6
	Swin-L (TTA)	v	55.6±0.05	77.3	61.8	45.7	59.6
	Swin-L-CLIP	2	56.6±0.4	79.2	63.0	45.6	60.3
	Swin-L-CLIP	5	56.3±0.3	78.4	62.5	45.6	59.7

We also implement the clip-tracking strategy [13] to conduct per-clip inference. We experiment with different clip-length (T) settings on both datasets. Table 4 compares the results. All per-clip results are also computed by averaging multiple runs. On YTVIS2019 dataset, per-clip inference leads to slightly worse results. However, on the YTVIS2021 dataset, per-clip inference exhibits better results. We conjecture that better results are potentially related to the almost doubled number of instances in YTVIS 2021 version dataset. With longer clip length and more instances, the inference gets more challenging when associating across instances. This will be further investigated and mitigated in the future.

However, per-clip inference increases the variances of the results. Especially, with $T = 2$, the variance is doubled on YTVIS2021 dataset and tripled on YTVIS2019 dataset.